Available online at www.sciencedirect.com
ScienceDirect
Physica C 456 (2007) 45–53
PHYSICA C
www.elsevier.com/locate/physc

Review

Superconducting properties of MgB_2 from first principles

A. Floris [a,b,*], A. Sanna [b], M. Lüders [c], G. Profeta [d], N.N. Lathiotakis [a], M.A.L. Marques [e], C. Franchini [b], E.K.U. Gross [a], A. Continenza [d], S. Massidda [b]

[a] *Institut für Theoretische Physik, Freie Universität Berlin, Arnimallee 14, D-14195 Berlin, Germany*
[b] *INFM SLACS, Sardinian Laboratory for Computational Materials Science, Dipartimento di Scienze Fisiche, Università degli Studi di Cagliari, S.P. Monserrato-Sestu km 0.700, I-09124 Monserrato (Cagliari), Italy*
[c] *Daresbury Laboratory, Warrington WA4 4AD, United Kingdom*
[d] *CNISM, Dipartimento di Fisica, Università degli Studi di L'Aquila, I-67010 Coppito (L'Aquila), Italy*
[e] *Departamento de Fsica, Universidade de Coimbra, Rua Larga, 3004-516 Coimbra, Portugal*

Received 23 January 2007; accepted 27 January 2007
Available online 13 February 2007

Abstract

The discovery of superconductivity in MgB_2, with a rather high transition temperature, has triggered a large number of theoretical and experimental investigations on important issues such as, e.g., the role of gap anisotropy over the Fermi surface (multi-gap superconductivity). We report here the results obtained in this compound using the density functional theory for superconductors, recently proposed by the authors. Without invoking any adjustable parameters, such as μ^*, we obtain the transition temperature, the gaps, and the specific heat in very good agreement with experiment. Moreover, our calculations allow for a detailed study of how the phonon-mediated attraction and Coulomb repulsion act differently on σ and π states, thereby stabilizing the observed superconducting phase.

PACS: 74.25.Jb; 74.25.Kc; 74.20.−z; 74.70.Ad; 71.15.Mb

Keyword: Superconductivity

Contents

* Corresponding author. Address: Institut für Theoretische Physik, Freie Universität Berlin, Arnimallee 14, D-14195 Berlin, Germany. Tel.: +49 30 838 53029; fax: +49 30 838 55258.
E-mail address: afloris@physik.fu-berlin.de (A. Floris).

0921-4534/$ - see front matter © 2007 Elsevier B.V. All rights reserved.
doi:10.1016/j.physc.2007.01.026

1. Introduction

Among the rather peculiar properties of MgB_2, the presence of two superconducting gaps at the Fermi level attracted strongly the attention of the scientific community. While in fact two-band or, more generally, multi-band superconductivity has long been known [1] to favor a high critical temperature, such a property was never observed in nature to the extent and clarity shown by MgB_2. On the theoretical side, most of calculations to date are based on the Eliashberg theory [2]. While in the latter the e–ph interaction is properly described in the spirit of Migdal's theorem, the effects of the e–e Coulomb repulsion are more difficult to account for in the Eliashberg approach: In most practical applications, the renormalized Coulomb pseudopotential μ^* is treated as an adjustable parameter, usually chosen as to reproduce the experimental T_c. The authors have recently extended the density functional theory, a very successful standard in normal state electronic structure calculations, to deal with the superconducting state (SCDFT). Unlike in Eliashberg based calculations, within SCDFT there are no adjustable parameters, and the critical temperature is the result of a true ab initio calculation. The difficulties hindered in an ab initio theory of the (phonon mediated) superconductivity arise from the fact that it must properly account for two strong and opposite effects, namely the phonon mediated attraction (denoted "e–ph" in the following) and the direct Coulomb repulsion (denoted "e–e") between the electrons. However, SCDFT theory turned out to be able to treat superconductors with a wide range of couplings, as shown by several investigations [3]. MgB_2 is surely one of its most interesting applications, owing to its unusual superconducting properties and its extraordinary high critical temperature.

In this work, we show how many approximations usually adopted in conventional low-T_c materials, for both the e–e and e–ph interactions (e.g. single order parameter, isotropic average of the interactions, or approximated screening of the direct Coulomb interaction between electrons) do not hold in MgB_2, resulting in wrong predictions of the superconducting properties that depart from the experimental results.

The paper is organized as follows: In Section 2 we summarize the main features of the method used; in Section 3 we describe in detail our computational approach and finally, in Section 4, we present and discuss our results.

2. Density functional theory for superconductors (SCDFT)

Density functional theory (DFT) [4] has enjoyed increasing popularity as a reliable and relatively inexpensive tool to describe real materials. Before turning to the problem of superconductivity, it is instructive to reconsider how magnetic systems are usually treated in a density functional approach. The Hohenberg–Kohn (HK) theorem [5] states that all observables, in particular also the magnetization, are functionals of the electronic density *alone*. However, even an approximate form of the magnetization functional is extremely hard to find, and, in practice, one chooses a different approach to this problem. The task can be vastly simplified by treating the magnetization density $\mathbf{m}(\mathbf{r})$, i.e., the order parameter of the magnetic state, as an additional density in the density functional framework. An auxiliary field – here a magnetic field $\mathbf{B}_{\mathrm{ext}}(\mathbf{r})$ – is introduced, which couples to $\mathbf{m}(\mathbf{r})$ and breaks the corresponding (rotational) symmetry of the Hamiltonian. In other words, it drives the system into a magnetically ordered state. The ground-state magnetization density is determined by minimizing the total energy functional (free energy functional for finite temperature calculations) with respect to both the normal density and the magnetization density. The resulting magnetization determines the effective magnetic field into the material. If a magnetic ground state exists, the order parameter will be non-zero even after the auxiliary perturbation is switched off again. Within this approach, much simpler approximations to the xc functional (now functional of two densities) can be found with satisfactory results when compared with the experiments. This idea forms the basis of the local spin density approximation and, likewise, of current density functional theory [6,7].

In the same spirit Oliveira et al. [8] formulated the density functional theory for superconductors. Here the order parameter is the so-called anomalous density,

$$\chi(\mathbf{r},\mathbf{r}') = \langle \hat{\Psi}_{\uparrow}(\mathbf{r})\hat{\Psi}_{\downarrow}(\mathbf{r}')\rangle, \tag{1}$$

and the corresponding potential is the non-local pairing potential $\Delta(\mathbf{r},\mathbf{r}')$. It can be interpreted as an external pairing field, induced by an adjacent superconductor via the proximity effect. Again, this external field only acts to break the symmetry (here the gauge symmetry) of the system, and is set to zero at the end of the calculation. As in the case of magnetism, the order parameter will be sustained by the self-consistent effective pairing field, if the system wants to be superconducting.

The formalism outlined so far captures, in principle, all electronic degrees of freedom. To describe conventional, phonon-mediated, superconductors, also the electron–phonon interaction has to be taken into account. In the weak coupling limit, this phonon-mediated interaction can be added as an additional BCS-type interaction. However, in order to treat also strong electron–phonon coupling, the electronic and the nuclear degrees of freedom have to be treated on equal footing. This can be achieved by a multi-component DFT, based on both the electronic density and the nuclear density [9]. The starting point is the full electron–ion Hamiltonian

$$\widehat{H} = \widehat{T}^{\mathrm{e}} + \widehat{U}^{\mathrm{ee}} + \widehat{T}^{\mathrm{n}} + \widehat{U}^{\mathrm{nn}} + \widehat{U}^{\mathrm{en}}, \tag{2}$$

where $\widehat{T}^{\mathrm{e}}$ represents the electronic kinetic energy, $\widehat{U}^{\mathrm{ee}}$ the electron–electron interaction, $\widehat{T}^{\mathrm{n}}$ the nuclear kinetic energy, and $\widehat{U}^{\mathrm{nn}}$ the Coulomb repulsion between the nuclei.

The interaction between the electrons and the nuclei is described by the term

$$\widehat{U}^{\mathrm{en}} = -\sum_{\sigma} \int \mathrm{d}^3 r \int \mathrm{d}^3 R \hat{\Psi}^{\dagger}_{\sigma}(\mathbf{r}) \hat{\Phi}^{\dagger}(\mathbf{R}) \frac{Z}{|\mathbf{r}-\mathbf{R}|} \hat{\Phi}(\mathbf{R}) \hat{\Psi}_{\sigma}(\mathbf{r}), \tag{3}$$

where $\hat{\Psi}_{\sigma}(\mathbf{r})$ and $\hat{\Phi}(\mathbf{R})$ are respectively electron and nuclear field operators. (For simplicity we assume the nuclei to be identical, and we neglect the nuclear spin degrees of freedom. The extension of this framework to a more general case is straightforward.) Note that there is no external potential in the Hamiltonian. In addition to the normal and anomalous electronic densities, we also include the diagonal of the nuclear density matrix [46]

$$\Gamma(\underline{\mathbf{R}}) = \left\langle \hat{\Phi}^{\dagger}(\mathbf{R}_1) \cdots \hat{\Phi}^{\dagger}(\mathbf{R}_N) \hat{\Phi}(\mathbf{R}_N) \cdots \hat{\Phi}(\mathbf{R}_1) \right\rangle \tag{4}$$

In order to formulate a Hohenberg–Kohn theorem for this system, we introduce a set of three potentials, which couple to the three densities described above. Since the electron–nuclear interaction, which in normal DFT constitutes the external potential, is treated explicitly in this formalism, it is *not* part of the external potential. The nuclear Coulomb interaction $\widehat{U}^{\mathrm{nn}}$ already has the form of an external many-body potential, coupling to $\Gamma(\underline{\mathbf{R}})$, and for the sake of the Hohenberg–Kohn theorem, this potential will be allowed to take the form of an arbitrary N-body potential. All three external potentials are merely mathematical devices, required to formulate a Hohenberg–Kohn theorem. At the end of the derivation they will be set to zero (in case of the external electronic and pairing potentials) and to the nuclear Coulomb interaction (for the external nuclear many-body potential).

As usual, the Hohenberg–Kohn theorem guarantees a one-to-one mapping between the set of the densities $\{n(\mathbf{r}), \chi(\mathbf{r},\mathbf{r}'), \Gamma(\underline{\mathbf{R}})\}$ in thermal equilibrium and the set of their conjugate potentials $\{v^{\mathrm{e}}_{\mathrm{ext}}(\mathbf{r}) - \mu, \Delta_{\mathrm{ext}}(\mathbf{r},\mathbf{r}'), v^{\mathrm{n}}_{\mathrm{ext}}(\underline{\mathbf{R}})\}$. As a consequence, all the observables are functionals of the set of densities. Finally, it assures that the grand canonical potential,

$$\begin{aligned}\Omega[n,\chi,\Gamma] = F[n,\chi,\Gamma] &+ \int \mathrm{d}^3 r n(\mathbf{r}) \left[v^{\mathrm{e}}_{\mathrm{ext}}(\mathbf{r}) - \mu\right] \\ &- \int \mathrm{d}^3 r \int \mathrm{d}^3 r' \left[\chi(\mathbf{r},\mathbf{r}') \Delta^*_{\mathrm{ext}}(\mathbf{r},\mathbf{r}') + \mathrm{h.c.}\right] \\ &+ \int \mathrm{d}^3 \underline{R} \Gamma(\underline{\mathbf{R}}) v^{\mathrm{n}}_{\mathrm{ext}}(\underline{\mathbf{R}})\end{aligned} \tag{5}$$

is minimized by the equilibrium densities. We use the notation $A[f]$ to denote that A is a functional of f. The functional $F[n,\chi,\Gamma]$ is universal, in the sense that it does not depend on the external potentials, and is defined by

$$\begin{aligned}F[n,\chi,\Gamma] = T^{\mathrm{e}}[n,\chi,\Gamma] + T^{\mathrm{n}}[n,\chi,\Gamma] + U^{\mathrm{en}}[n,\chi,\Gamma] \\ + U^{\mathrm{ee}}[n,\chi,\Gamma] - \frac{1}{\beta} S[n,\chi,\Gamma],\end{aligned} \tag{6}$$

where S is the entropy of the system,

$$S[n,\chi,\Gamma] = -\mathrm{Tr}\{\hat{\rho}_0[n,\chi,\Gamma] \ln(\hat{\rho}_0[n,\chi,\Gamma])\}. \tag{7}$$

The proof of the theorem follows closely the proof of the Hohenberg–Kohn theorem at finite temperatures [10].

2.1. Kohn–Sham system

In standard DFT one normally defines a Kohn–Sham system, i.e., a non-interacting system chosen such that it has the same ground-state density as the interacting one. In our formalism, the Kohn–Sham system consists of non-interacting (superconducting) electrons, and *interacting* nuclei. It is described by the thermodynamic potential [cf. Eq. (5)]

$$\begin{aligned}\Omega_{\mathrm{s}}[n,\chi,\Gamma] = F_{\mathrm{s}}[n,\chi,\Gamma] &+ \int \mathrm{d}^3 r n(\mathbf{r}) \left[v^{\mathrm{e}}_{\mathrm{s}}(\mathbf{r}) - \mu_{\mathrm{s}}\right] \\ &- \int \mathrm{d}^3 r \int \mathrm{d}^3 r' \left[\chi(\mathbf{r},\mathbf{r}') \Delta^*_{\mathrm{s}}(\mathbf{r},\mathbf{r}') + \mathrm{h.c.}\right] \\ &+ \int \mathrm{d}^3 \underline{R} \Gamma(\underline{\mathbf{R}}) v^{\mathrm{n}}_{\mathrm{s}}(\underline{\mathbf{R}}),\end{aligned} \tag{8}$$

where F_{s} if the counterpart of (6) for the Kohn–Sham system, i.e.,

$$F_{\mathrm{s}}[n,\chi,\Gamma] = T^{\mathrm{e}}_{\mathrm{s}}[n,\chi,\Gamma] + T^{\mathrm{n}}_{\mathrm{s}}[n,\chi,\Gamma] - \frac{1}{\beta} S_{\mathrm{s}}[n,\chi,\Gamma]. \tag{9}$$

Here $T^{\mathrm{e}}_{\mathrm{s}}[n,\chi,\Gamma]$, $T^{\mathrm{n}}_{\mathrm{s}}[n,\chi,\Gamma]$, and $S_{\mathrm{s}}[n,\chi,\Gamma]$ are the electronic and nuclear kinetic energies and the entropy of the Kohn–Sham system, respectively. From Eq. (8) it is clear that the Kohn–Sham nuclei interact with each other through the N-body potential $v^{\mathrm{n}}_{\mathrm{s}}(\underline{\mathbf{R}})$, while they do not interact with the electrons.

The Kohn–Sham potentials, which are derived in analogy to normal DFT, include the external fields, Hartree, and exchange-correlation terms. The latter account for all many-body effects of the electron–electron and electron–nuclear interactions and are, as usual, given by the respective functional derivatives of the xc energy functional defined through

$$F[n,\chi,\Gamma] = F_{\mathrm{s}}[n,\chi,\Gamma] + F_{\mathrm{xc}}[n,\chi,\Gamma] + E^{\mathrm{ee}}_{\mathrm{H}}[n,\chi] + E^{\mathrm{en}}_{\mathrm{H}}[n,\Gamma]. \tag{10}$$

There are two contributions to $E^{\mathrm{ee}}_{\mathrm{H}}$, one originating from the electronic Hartree potential, and the other from the anomalous Hartree potential

$$E^{\mathrm{ee}}_{\mathrm{H}}[n,\chi] = \frac{1}{2} \int \mathrm{d}^3 r \int \mathrm{d}^3 r' \frac{n(\mathbf{r}) n(\mathbf{r}')}{|\mathbf{r}-\mathbf{r}'|} + \int \mathrm{d}^3 r \int \mathrm{d}^3 r' \frac{|\chi(\mathbf{r},\mathbf{r}')|^2}{|\mathbf{r}-\mathbf{r}'|}. \tag{11}$$

Finally, $E^{\mathrm{en}}_{\mathrm{H}}$ denotes the electron–nuclear Hartree energy

$$E^{\mathrm{en}}_{\mathrm{H}}[n,\Gamma] = -Z \sum_{\alpha} \int \mathrm{d}^3 r \int \mathrm{d}^3 \underline{R} \frac{n(\mathbf{r}) \Gamma(\underline{\mathbf{R}})}{|\mathbf{r}-\mathbf{R}_{\alpha}|}. \tag{12}$$

The problem of minimizing the Kohn–Sham grand canonical potential (8) can be transformed into a set of three differential equations that have to be solved self-consistently: One equation for the nuclei, which resembles the familiar nuclear Born–Oppenheimer equation, and two coupled equations which describe the electronic degrees of freedom and have the algebraic structure of the Bogoliubov-de Gennes [11] equations.

The Kohn–Sham equation for the nuclei has the form

$$\left[-\sum_{\alpha}\frac{\nabla_{\alpha}^2}{2M}+v_{\mathrm{s}}^{\mathrm{n}}(\underline{\mathbf{R}})\right]\Phi_{\mathrm{l}}(\underline{\mathbf{R}})=\mathscr{E}_{\mathrm{l}}\Phi_{\mathrm{l}}(\underline{\mathbf{R}}). \tag{13}$$

We emphasize that the Kohn–Sham Eq. (13) does not rely on any approximation and is, in principle, exact. In practice, however, the unknown effective potential for the nuclei is approximated by the Born–Oppenheimer surface. As already mentioned, we are interested in solids at relatively low temperature, where the nuclei perform small amplitude oscillations around their equilibrium positions. In this case, we can expand $v_{\mathrm{s}}^{\mathrm{n}}[n,\chi,\Gamma]$ in Taylor series around the equilibrium positions, and transform the nuclear degrees of freedom into collective (phonon) coordinates. In harmonic order, the nuclear Kohn–Sham Hamiltonian then reads

$$\hat{H}_{\mathrm{s}}^{\mathrm{ph}}=\sum_{\lambda,\mathbf{q}}\Omega_{\lambda,\mathbf{q}}\left[\hat{b}_{\lambda,\mathbf{q}}^{\dagger}\hat{b}\dagger_{\lambda,\mathbf{q}}+\frac{1}{2}\right], \tag{14}$$

where $\Omega_{\lambda,\mathbf{q}}$ are the phonon eigenfrequencies, and $\hat{b}_{\lambda,\mathbf{q}}^{\dagger}$ creates a phonon in branch λ and at wave-vector $\mathbf{q}$. Note that the phonon eigenfrequencies are functionals of the set of densities $\{n,\chi,\Gamma\}$, and can therefore be affected by the superconducting order parameter.

The Kohn–Sham Bogoliubov-de Gennes (KS-BdG) equations read

$$\left[-\frac{\nabla^2}{2}+v_{\mathrm{s}}^{\mathrm{e}}(\mathbf{r})-\mu\right]u_{n\mathbf{k}}(\mathbf{r})+\int \mathrm{d}^3r'\Delta_{\mathrm{s}}(\mathbf{r},\mathbf{r}')v_{n\mathbf{k}}(\mathbf{r}')=\tilde{E}_{n\mathbf{k}}u_{n\mathbf{k}}(\mathbf{r}), \tag{15a}$$

$$-\left[-\frac{\nabla^2}{2}+v_{\mathrm{s}}^{\mathrm{e}}(\mathbf{r})-\mu\right]v_{n\mathbf{k}}(\mathbf{r})+\int \mathrm{d}^3r'\Delta_{\mathrm{s}}^{*}(\mathbf{r},\mathbf{r}')u_{n\mathbf{k}}(\mathbf{r}')=\tilde{E}_{n\mathbf{k}}v_{n\mathbf{k}}(\mathbf{r}), \tag{15b}$$

where $u_{n\mathbf{k}}(\mathbf{r})$ and $v_{n\mathbf{k}}(\mathbf{r})$ are the particle and hole amplitudes. This equation is very similar to the Kohn–Sham equations in the OGK formalism [8]. However, in the present formulation the lattice potential is not considered an external potential but enters via the electron–ion Hartree term. Furthermore, our exchange-correlation potentials depend on the nuclear density matrix, and therefore on the phonons. Although Eqs. (13) and (15) have the structure of static mean-field equations, they contain, in principle, all correlation and retardation effects through the exchange-correlation potentials.

These KS-BdG equations can be simplified by the so-called decoupling approximation [12,14], which corresponds to the following ansatz for the particle and hole amplitudes:

$$u_{n\mathbf{k}}(\mathbf{r})\approx u_{n\mathbf{k}}\varphi_{n\mathbf{k}}(\mathbf{r});\quad v_{n\mathbf{k}}(\mathbf{r})\approx v_{n\mathbf{k}}\varphi_{n\mathbf{k}}(\mathbf{r}), \tag{16}$$

where the wave functions $\varphi_{n\mathbf{k}}(\mathbf{r})$ are the solutions of the normal Schrödinger equation. In this way the eigenvalues in Eq. (15) become $\tilde{E}_{n\mathbf{k}}=\pm E_{n\mathbf{k}}$, where

$$E_{n\mathbf{k}}=\sqrt{\xi_{n\mathbf{k}}^2+|\Delta_{n\mathbf{k}}|^2}, \tag{17}$$

and $\xi_{n\mathbf{k}}=\epsilon_{n\mathbf{k}}-\mu$. This form of the eigenenergies allows us to interpret the pair potential $\Delta_{n\mathbf{k}}$ as the gap function of the superconductor. Furthermore, the coefficients $u_{n\mathbf{k}}$ and $v_{n\mathbf{k}}$ are given by simple expressions within this approximation

$$u_{n\mathbf{k}}=\frac{1}{\sqrt{2}}\mathrm{sgn}(\tilde{E}_{n\mathbf{k}})\mathrm{e}^{\mathrm{i}\Phi_{n\mathbf{k}}}\sqrt{1+\frac{\xi_{n\mathbf{k}}}{\tilde{E}_{n\mathbf{k}}}}, \tag{18a}$$

$$v_{n\mathbf{k}}=\frac{1}{\sqrt{2}}\sqrt{1-\frac{\xi_{n\mathbf{k}}}{\tilde{E}_{n\mathbf{k}}}}. \tag{18b}$$

Finally, the matrix elements $\Delta_{n\mathbf{k}}$ are defined as

$$\Delta_{n\mathbf{k}}=\int \mathrm{d}^3r\int \mathrm{d}^3r'\varphi_{n\mathbf{k}}^{*}(\mathbf{r})\Delta_{\mathrm{s}}(\mathbf{r},\mathbf{r}')\varphi_{n\mathbf{k}}(\mathbf{r}'), \tag{19}$$

and $\Phi_{n\mathbf{k}}$ is the phase $\mathrm{e}^{\mathrm{i}\Phi_{n\mathbf{k}}}=\Delta_{n\mathbf{k}}/|\Delta_{n\mathbf{k}}|$. The normal and the anomalous densities can then be easily obtained from

$$n(\mathbf{r})=\sum_{n\mathbf{k}}\left[1-\frac{\xi_{n\mathbf{k}}}{E_{n\mathbf{k}}}\tanh\left(\frac{\beta}{2}E_{n\mathbf{k}}\right)\right]|\varphi_{n\mathbf{k}}(\mathbf{r})|^2, \tag{20a}$$

$$\chi(\mathbf{r},\mathbf{r}')=\frac{1}{2}\sum_{n\mathbf{k}}\frac{\Delta_{n\mathbf{k}}}{E_{n\mathbf{k}}}\tanh\left(\frac{\beta}{2}E_{n\mathbf{k}}\right)\varphi_{n\mathbf{k}}(\mathbf{r})\varphi_{n\mathbf{k}}^{*}(\mathbf{r}'). \tag{20b}$$

2.2. Gap equation

Within the decoupling approximation outlined above, a major effort was devoted to find an expression for the effective pairing potential. The actual approximations for the xc functionals turn out to be not explicit functionals of the densities, but rather functionals of the potentials, still being implicit functionals of the density. Therefore the task of calculating the effective pair potential is to solve the nonlinear functional equation

$$\Delta_{\mathrm{s},n\mathbf{k}}=\Delta_{\mathrm{xc},n\mathbf{k}}[\mu,\Delta_{\mathrm{s}}]. \tag{21}$$

In the vicinity of the critical temperature, where the order parameter and hence the pairing potential vanishes, this equation can be linearized, giving rise to a BCS-like gap equation:

$$\breve{\Delta}_{n\mathbf{k}}=-\frac{1}{2}\sum_{n'\mathbf{k}'}\mathscr{F}_{\mathrm{Hxc}\,n\mathbf{k},n'\mathbf{k}'}[\mu]\frac{\tanh\left(\frac{\beta}{2}\xi_{n'\mathbf{k}'}\right)}{\xi_{n'\mathbf{k}'}}\breve{\Delta}_{n'\mathbf{k}'}, \tag{22}$$

where the anomalous Hartree exchange-correlation kernel of the homogeneous integral equation reads

$$\mathscr{F}_{\mathrm{Hxc}\,n\mathbf{k},n'\mathbf{k}'}[\mu]=-\left.\frac{\delta\Delta_{\mathrm{Hxc}\,n\mathbf{k}}}{\delta\chi_{n'\mathbf{k}'}}\right|_{\chi=0}=\left.\frac{\delta^2(E_{\mathrm{H}}^{\mathrm{ee}}+F_{\mathrm{xc}})}{\delta\chi_{n\mathbf{k}}^{*}\delta\chi_{n'\mathbf{k}'}}\right|_{\chi=0}. \tag{23}$$

Although this linearized gap equation is strictly valid only in the vicinity of the transition temperature, we use the same kernel $\mathscr{F}_{\mathrm{Hxc}}$ in a partially linearized equation, that has the same structure but contains the energies $E_{n\mathbf{k}}$ in place of the $\xi_{n\mathbf{k}}$, also at lower temperatures. Furthermore, we split the kernel into a purely diagonal part $\mathscr{Z}$ and a truly off-diagonal part $\mathscr{K}$,

$$\Delta_{n\mathbf{k}} = -\mathscr{Z}_{n\mathbf{k}}\Delta_{n\mathbf{k}} - \frac{1}{2}\sum_{n'\mathbf{k}'} \mathscr{K}_{n\mathbf{k},n'\mathbf{k}'} \frac{\tanh\left(\frac{\beta}{2}E_{n'\mathbf{k}'}\right)}{E_{n'\mathbf{k}'}}\Delta_{n'\mathbf{k}'}. \tag{24}$$

Eq. (24) is the central equation of the DFT for superconductors. The kernel $\mathscr{K}$ consists of two contributions $\mathscr{K} = \mathscr{K}^{\mathrm{e-ph}} + \mathscr{K}^{\mathrm{e-e}}$, representing the effects of the e–ph and of the e–e interactions, respectively. The diagonal term $\mathscr{Z}$ plays a similar role as the renormalization term in the Eliashberg equations. Explicit expressions of $\mathscr{K}^{\mathrm{e-ph}}$ and $\mathscr{Z}$, which are the results of the approximate functionals implemented, are given in Eqs. (9) and (11) of Ref. [13] respectively. These two terms involve the e–ph coupling matrix, while $\mathscr{K}^{\mathrm{e-e}}$ contains the matrix elements of the screened Coulomb interaction (the explicit expression is given below). Eq. (24) has the same structure as the BCS gap equation, with the kernel $\mathscr{K}$ replacing the model interaction of BCS theory. This similarity allows us to interpret the kernel as an effective interaction responsible for the binding of the Cooper pairs. As already mentioned, Eq. (24) is not a mean-field equation (as in BCS theory), since it contains correlation effects via the SC exchange-correlation functional entering $\mathscr{K}$ and $\mathscr{Z}$. Furthermore, it has the form of a static equation – i.e., it does not depend *explicitly* on the frequency – and therefore has a simpler structure (and computationally more manageable) than the Eliashberg equations. However, this certainly does not imply that retardation effects are absent from the theory. Once again, retardation effects enter through the xc functional, as explained in Refs. [12,13].

3. Computational details

The solution of Eq. (24) first requires the calculation of the normal state band structure $\epsilon_{n\mathbf{k}}$ of the material, the phonon spectrum $\omega_{\mathbf{q}\nu}$, and the e–ph and Coulomb matrix elements (ME) with respect to the Bloch functions.

The eigenvalues $\epsilon_{n\mathbf{k}}$ are calculated over a few hundreds of **k**-points in the irreducible wedge of the Brillouin zone, and successively interpolated on a regular grid of 128^3 points, according to the scheme described in Refs. [15,16]. Where not explicitly said, the e–ph coupling was included through the four, band resolved, Eliashberg functions $\alpha^2F_{n,n'}(\omega)$ previously employed within a two-band Eliashberg scheme by Golubov et al. [36], where

$$\alpha^2F_{nn'}(\omega) = \frac{1}{N_n(E_{\mathrm{F}})}\sum_{\mathbf{k},\mathbf{k}',\nu}\left|g^{nn'}_{\mathbf{k},\mathbf{k}',\nu}\right|^2 \delta(\epsilon_{n\mathbf{k}} - E_{\mathrm{F}}) \times \delta(\epsilon_{n'\mathbf{k}'} - E_{\mathrm{F}})\delta(\omega - \omega_{\mathbf{k}'-\mathbf{k},\nu}). \tag{25}$$

Here (n, $n' = \sigma$, π) and $N_n(E_{\mathrm{F}})$ is the partial density of states at Fermi level. Our procedure keeps the fundamental distinction between σ and π gaps, analogously to most of the Eliashberg calculations reported to date. By using the $\alpha^2F_{n,n'}(\omega)$, the e–ph interaction is averaged over **k** and **k**′ at the FS, which may have a small, but non-negligible effect. We define the bands crossing the FS to be of σ character if they are contained in a cylinder of basis radius 1/4 of a reciprocal lattice vector, and of π character otherwise. Away from the Fermi surface this distinction is meaningless but harmless, as the phonon terms die off quickly and the Coulomb term is independent of this distinction.

In a new fully anisotropic implementation of the code, an $n\mathbf{k}$, $n'\mathbf{k}'$-resolved e–ph interaction was included in the SCDFT formalism. In this case, and contrary to the previous approach, we did not assume any specific form for the el–ph and e–e interaction. However, the multi-band nature of MgB_2 emerges in a completely natural way: We find that the solutions of the Eq. (24) at each temperature clusterize into two distinct gaps with the same critical temperature (see below). The phonon spectrum and the e–ph ME were calculated via density functional perturbation theory [37], within the planewave-pseudopotential method [38]. The calculation was performed at the experimental lattice constants within the GGA approximation [39] with ultrasoft pseudopotentials [40]. An energy cut-off of 25 Ry for the wavefunctions, 300 Ry for the charge density and a $24\times24\times22$ Monkhorst–Pack **k**-point grid were sufficient to achieve very good convergence of the phonon spectrum and the e–ph ME $|g^{nn'}_{\mathbf{k},\mathbf{k}',\nu}|^2$. Phonon frequencies and e–ph ME were calculated on the irreducible set of a regular mesh of 8^3 **q**-points, the el–ph ME on a grid of 24^3 **k**-points and the Coulomb ME on a $9^3\times9^3$ mesh for **k** and **k**′-points. The $\omega_{\mathbf{q}\nu}$ were interpolated on a grid of 128^3 **q**-points following the same scheme employed for the KS energies $\epsilon_{n\mathbf{k}}$ [15,16]. The $|g^{nn'}_{\mathbf{k},\mathbf{k}',\nu}|^2$ were interpolated on a grid of 20^3 **q**-points using a six-dimensional Fast Fourier Transform technique. The corresponding total e–ph coefficient obtained is $\lambda = 0.71$. Band-resolved values are: $\lambda_{\sigma\sigma} = 0.83$; $\lambda_{\sigma\pi} = 0.22$; $\lambda_{\pi\sigma} = 0.16$; $\lambda_{\pi\pi} = 0.28$. Our calculated $\lambda_{\sigma\sigma}$, $\lambda_{\pi\pi}$ and λ, are significantly lower than the values $\lambda_{\sigma\sigma} = 1.017$, $\lambda_{\pi\pi} = 0.45$ and $\lambda = 0.87$ obtained in Refs. [36,19], but basically in agreement with calculations by Bohnen et al. [20]: $\lambda = 0.73$; Liu et al. [33]: $\lambda = 0.77$; Choi et al.: [29] = $\lambda = 0.73$; Singh: [32] = $\lambda = 0.68$.

The comparison of the calculated density of states with the specific heat experiments by Putti et al. [26] leads to $\lambda = 0.8$, larger than our results, while $\lambda = 0.61$ is obtained from the measurements of Junod's group [41]. The de Haas–van Alphen experiments lead, for the σ sheets, to values of $\lambda_\sigma = \lambda_{\sigma\sigma} + \lambda_{\sigma\pi}$ in the range from 0.91 and 1.2, somehow in between our calculated λ's and those by Kong et al. [19] and Golubov et al. [36]. We conclude therefore that the comparison between calculated e–ph couplings and experiment does not provide, at the moment, an univocal answer (see also the discussion below).

SCDFT allows to treat on the same footing the e–ph and the screened e–e interactions. We calculated the screened Coulomb ME with respect to the Bloch functions, for the whole energy range of relevant valence and conduction states. The different nature of σ and π bands and in particular the highly localized character of the former, strongly calls for the use of a non-diagonal screening, including local field effects. In order to describe properly these effects, that are very important to achieve a good agreement with the experiment, we calculated the static RPA dielectric matrix (DM) $\epsilon^{-1}(\boldsymbol{q},\boldsymbol{G},\boldsymbol{G}')$, using the pseudopotential-based SELF code [42]. The explicit expression of the kernel $\mathscr{K}^{\mathrm{e-e}}$ in reciprocal space reads

$$\mathscr{K}^{\mathrm{e-e}}_{n\mathbf{k},n'\mathbf{k}'} = \sum_{\boldsymbol{G},\boldsymbol{G}'} \epsilon^{-1}(\boldsymbol{q},\boldsymbol{G},\boldsymbol{G}') \times 4\pi \frac{\langle n'\boldsymbol{k}'|e^{i(\boldsymbol{q}+\boldsymbol{G})\cdot\boldsymbol{r}}|n\mathbf{k}\rangle\langle n\mathbf{k}|e^{-i(\boldsymbol{q}+\boldsymbol{G}')\cdot\boldsymbol{r}'}|n'\mathbf{k}'\rangle}{|\boldsymbol{q}+\boldsymbol{G}||\boldsymbol{q}+\boldsymbol{G}'|}, \quad (26)$$

The SC gap function is extremely peaked around the Fermi surface, whereas at higher energies is rather smooth (and negative, due to the e–e interaction). This implies that a converged solution of Eq. (24) needs a denser **k**-points sampling around E_F, and coarser elsewhere. This highly non-uniform mesh of the BZ is realized with 13×10^3 and 1000 independent **k**-points for bands crossing and not crossing the Fermi level respectively. Finally, 15–20 self-consistent iterations were sufficient to achieve a complete convergence of the gap.

4. Results

The MgB_2 Fermi surface has several sheets with different orbital character (see e.g. Ref. [17]). In particular, the tubular structures with σ character are very strongly coupled to the E_{2g} phonon mode, corresponding to a B–B bond-stretching in the boron planes [17–20]. The π bands at the Fermi level form three-dimensional sheets.

The different orbital character of the two kinds of bands crossing the Fermi level and the separated Fermi surfaces originating from them is a remarkable feature of this compound. This results in the presence of two distinguishable gaps on the σ and π bands, as clearly demonstrated by several different experiments [21–28]. On the theoretical side, this system has been treated within the **k**-resolved Eliashberg theory [29,30], using a two-band scheme [31,33,36], with four e–ph spectral functions to represent the distinct couplings. Correspondingly, the anisotropy of the Coulomb interaction was only investigated within the two bands model, using a uniform [29,35], diagonal [34] and non-diagonal [36] $2\times2\mu^*$ matrix.

The ab initio nature of SCDFT allows to make some statements concerning the strength of the e–ph and the Coulomb interaction in MgB_2. Setting the Coulomb ME equal to zero, the SCDFT method, for this material, gives essentially the same gaps and T_c as the Eliashberg approach with $\mu^*=0$. This fact confirms the simple metals results shown in Table 1 of Ref. [12], and means that the two approaches, although in principle very different, treat the phonon contribution at the same level of approximation. Our fully anisotropic SCDFT calculation (including a corresponding $\lambda=0.71$ and RPA Coulomb ME), gives $T_c=22$ K, in strong disagreement with T_c^{exp}. On the other hand, it is worth to note that in Eliashberg based theoretical works, very different fitting values of μ^* are requested to reproduce T_c^{exp} in presence of the very different values of λ found in the literature. The latter are grouped essentially in two sets: $\lambda=0.87$ (Golubov et al. [36], Kong et al. [19]) and $\lambda\approx0.7$ (present work and Refs. [20,29,32]). The μ^* values can also be grouped in two sets: the $2\times2\mu^*_{nn'}$ matrix which corresponds to an isotropic $\mu^*=0.268$ (Ref. [36]), and the $\mu^*_{nn'}$ values which average to $\mu^*\approx0.12$ (Refs. [29,35]). Now, always assuming a two-band model calculation with respect to both the interactions, T_c^{exp} is reproduced either (i) using $\lambda\approx0.7$ and $\mu^*\approx0.12$ or (ii) using $\lambda=0.87$ and $\mu^*=0.268$. Our RPA Coulomb ME, averaged on the Fermi surface, give an unrenormalized pseudopotential $\mu=0.263$, in perfect agreement with the ab initio calculation of Moon et al. [35]. As we will see below, with these ME, the SCDFT T_c is in good agreement with T_c^{exp} only with $\lambda=0.87$. From this analysis, we believe that in the quantitative description of MgB_2 there are not fully understood aspects, related either to the values of the e–ph or of the renormalized Coulomb interaction. We then sketch two possible scenarios:

(1) Suppose that our (strong) RPA Coulomb ME and the fitting parameters $\mu^*_{nn'}$ of Ref. [36] properly describe the e–e repulsion. Then $\mu^*=0.12$ would be too low (or too strongly renormalized, as in Ref. [35]) and the value $\lambda\approx0.7$, although correctly calculated in most of the theoretical works, would not reproduce all the relevant features of the e–ph coupling in MgB_2 (producing a too low T_c in both SCDFT and Eliashberg approaches). The reason of this underestimate would be unclear at present.

(2) Conversely, suppose that the two-band e–ph interaction averaging to $\lambda\approx0.7$ captured all the MgB_2 e–ph physics. Then the value $\lambda=0.87$, our RPA Coulomb ME, the ME calculated in Ref. [35] and the $\mu^*_{nn'}$ of Ref. [36] would be too strong. In the case of our Coulomb ME this could be related, e.g., to a not enough elaborated screening (for this material). In the Eliashberg approach, only a matrix of $\mu^*_{nn'}$ averaging to a $\mu^*\approx0.12$ would then be able to reproduce T_c^{exp} [47].

As none of the two scenarios is more plausible than the other at present, we leave open the question of which are the correct physical values of the ME and in the following we present our two-band model calculation, which assumes the validity of scenario (1).

In Fig. 1 we plot the superconducting gap, as a function of (positive) energy distance from the Fermi energy, obtained including the screened Coulomb ME $\mathscr{K}^{\mathrm{e-e}}$ (Eq. (26)). The corresponding results slightly differ from the ones of Ref. [43], where the DM model of Hybertsen and Louie (HL) [44] including local fields was employed.

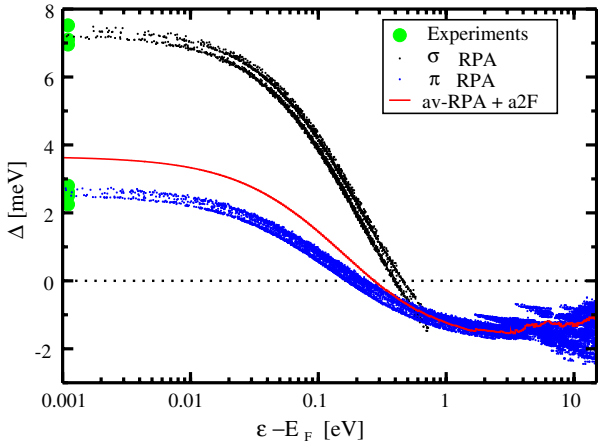

Fig. 1. Calculated superconducting gap of MgB_2 as a function of energy. In σ RPA, π RPA the Coulomb matrix elements are screened by an RPA dielectric matrix and the e–ph coupling is included via the band resolved $\alpha^2F_{nn'}(\omega)$. In av-RPA + $a2F(\omega)$ a completely isotropic calculation is performed, both for phononic and electronic terms.

Fig. 1 shows that the σ gap is defined only up to the energy of the top of the σ band and that both Δ_σ and Δ_π are anisotropic. This anisotropy results from the Coulomb potential matrix elements, and is roughly 0.4 meV, ≈6% of Δ_σ at the FS but much larger at high energy, where there are many bands with different orbital characters. The averages of Δ_σ and Δ_π at the Fermi level (7.3 meV and 2.6 meV, respectively) are in excellent agreement with experiment (7.1 meV and 2.9 meV) [24]. Both gaps change sign leading to the renormalization of the Coulomb interaction, which is a crucial condition to find superconductivity in the presence of the repulsive Coulomb interaction. In fact, our gap equation does not converge to a superconducting solution, unless all the electronic states in a large energy window are included. We see a striking difference between the anisotropic and completely isotropic solution (red line),[1] which will be discussed in detail later.

In Fig. 2 (panel (a)), the superconducting gaps are plotted versus temperature, together with a few recent experimental results. The agreement is striking: the values of T_c (36.5 K) and of Δ_σ and Δ_π at $T = 0$ K are very close to the experimental data. Moreover, the temperature behavior of both gaps, along with their strongly non-BCS behavior, are very well reproduced. Obviously, unlike calculations performed using Eliashberg theory, we do not reproduce exactly the experimental critical temperature, as our calculations are not fitted to match any experimental quantity. As discussed later (see Table 1), we see that the present values of Δ_σ, Δ_π and T_c are in better agreement with the experiment than to the ones of Ref. [43], meaning that the

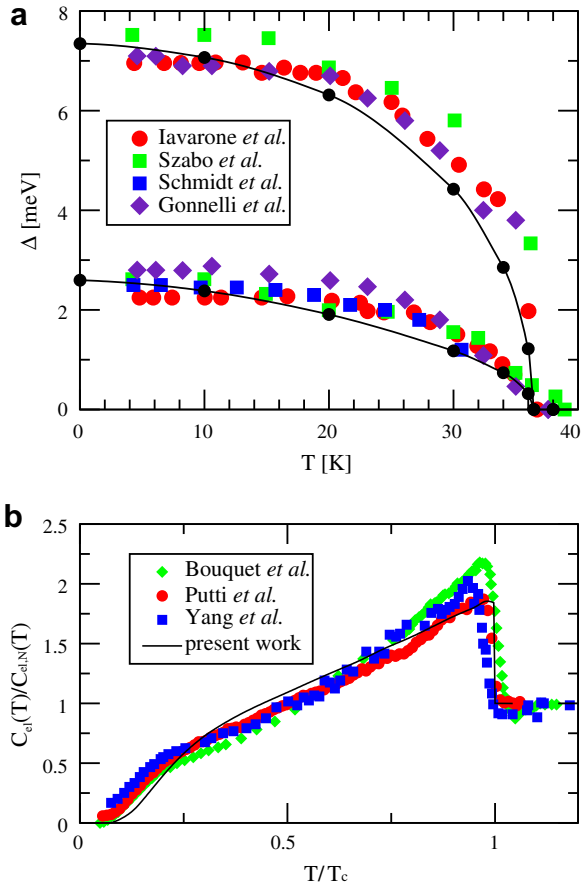

Fig. 2. Superconducting gaps at the FS and specific heat of MgB_2. Panel (a): Comparison between theoretical and experimental gap at the FS plotted as a function of temperature. The calculated gaps and T_c (36.5 K) are obtained without the use of any adjustable parameter. Panel (b): Experimental and calculated electronic specific heat, as a function of T/T_c.

ab initio calculation of the DM has a non-negligible effect on the gap, relative to the HL model for DM [44].

The full anisotropic calculation of the gap allows to evidence the intraband gap anisotropy, which is found to

Table 1
Summary of calculated T_c (K) and gaps (meV)

Coulomb e–e	$\alpha^2F_{nn'}(\omega)$			$\alpha^2F(\omega)$		
	T_c	Δ_σ	Δ_π	T_c	Δ_σ	Δ_π
RPA	36.5	7.3	2.6	20.8	3.8	3.8
av-RPA	50.2	9.4	1.5	20.8	3.7	
RPA-DIAG	30.0	5.9	2.2		–	
HL	34.1	6.8	2.5		–	
TF-ME	31.0	6.1	2.3		–	
exp	38.2	7.1	2.9		–	

Coulomb e–e: RPA = RPA dielectric matrix with local fields (LF); RPA-DIAG = RPA diagonal dielectric matrix (no LF); HL = model dielectric matrix from Ref. [44] (with LF); TF-ME = Thomas–Fermi screening; av-RPA = average of RPA ME (Eq. (27)). Experimental values are taken from Ref. [24].

[1] For interpretation of color in Figs. 1 and 3, the reader is referred to the web version of this article.

be $\Delta_\sigma^{\max}(E_F) - \Delta_\sigma^{\min}(E_F) = 0.8$ meV, $\Delta_\pi^{\max}(E_F) - \Delta_\pi^{\min}(E_F) = 1$ meV. Concerning the σ sheets, we find higher gap values in the smaller cylinders, whereas in the π sheets the gap is higher in the antibonding sheet than in the bonding. As expected, being the bonding bands more localized than the antibonding, both the e–ph and Coulomb ME are stronger in the former bands. In any case, the intraband anisotropy plays surely a minor role if compared with the interband anisotropy, confirming the validity of the two-band model in this material.

We also calculated the Kohn–Sham entropy as a function of temperature and, from its temperature derivative, the specific heat. In order to compare our results with experiments [26–28], we plot in Fig. 2 (panel (b)) the reduced specific heat versus temperature, normalized to T_c (using the corresponding experimental and calculated T_c values). Both the shape of the curve as well as the discontinuity at T_c are almost perfectly reproduced. We recall that the low temperature shoulder comes from the presence of the smaller π gap.

4.1. Screening and anisotropy of the interactions: influence on T_c

While the good agreement with experiment underlines the predictive power of our method, it is only one part of our investigation. Another important aspect is to gain further insight into the peculiar superconductivity of MgB_2. To this end, we performed several calculations using different approximations for the screened Coulomb interaction and including both a band-resolved (via $\alpha^2F_{nn'}(\omega)$) and isotropic (via $\alpha^2F(\omega)$) e–ph coupling. Our results are summarized in Table 1.

The anisotropy of the Coulomb interaction strongly affects T_c. Including in Eq. (24) the $\alpha^2F_{nn'}(\omega)$ and the averaged Coulomb interaction (denoted av-RPA):

$$\mathscr{K}^{\text{e–e}}_{\text{av}}(\epsilon,\epsilon') = \frac{1}{N(\epsilon)N(\epsilon')}\sum_{n\mathbf{k},n'\mathbf{k}'}\mathscr{K}^{\text{e–e}}_{n\mathbf{k},n'\mathbf{k}'}\delta(\epsilon_{n\mathbf{k}}-\epsilon)\delta(\epsilon_{n'\mathbf{k}'}-\epsilon') \tag{27}$$

we obtain $T_c = 50.2$ K, with the σ and π gaps being 9.4 meV and 1.5 meV, respectively. This test shows that the repulsion among σ states, stronger than within π and between σ and π, is crucial in achieving good agreement with experiment. It is interesting to notice that the averaging of the Coulomb matrix elements reduces the π gap, presumably by assigning it a larger repulsive term. Conversely, if we average also the e–ph spectral functions (using the isotropic $\alpha^2F(\omega)$), we obtain a single gap $\Delta = 3.7$ meV and the much lower $T_c = 20.8$ K, in agreement with the analysis of Ref. [33] and with a similar test carried out by Choi et al. [29]. Moreover, with an averaged e–ph interaction, we obtain a single gap also if the RPA anisotropic Coulomb interaction is included. This means that the Coulomb interaction alone is not able to induce a band anisotropy in the SC gap.

Of course, in the search for novel superconductors with higher transition temperatures, it would be desirable to keep the extremely strong e–ph coupling for σ states, while reducing the corresponding Coulomb interaction to that of more delocalized π states. Unfortunately, the two features are linked together, as both the strong e–ph coupling and the strong Coulomb repulsion derive from the covalent nature of the corresponding electronic states.

To push this analysis further, we plot, in the upper panel of Fig. 3, the energy dependence of the Coulomb contribution to Eq. (24) at $T \approx 0$ K, namely $\mathscr{K}^{\text{e–e}}_{n\mathbf{k},n'\mathbf{k}'}\Delta_{n'\mathbf{k}'}/(2E_{n'\mathbf{k}'}) \equiv \mathscr{K}^{\text{e–e}}_{n\mathbf{k},n'\mathbf{k}'}\chi_{n'\mathbf{k}'}$ against $\xi_{n'\mathbf{k}'} = \varepsilon_{n'\mathbf{k}'} - E_F$, for a few $\mathbf{k}$-points arbitrarily chosen on the Fermi surface. As $\chi_{n'\mathbf{k}'}$ goes to 0.5 on the Fermi surface, Fig. 3 shows the larger magnitude of the intraband σ–σ and π–π, relative to the interband σ–π matrix elements (see also Ref. [35]). The different behavior of the σ → π and π → σ terms results from the χ factor, as the matrix elements themselves are symmetric. Obviously, the σ–σ repulsive matrix elements are the strongest. The scattering of data for a given energy comes from the different orbital character of wavefunctions at $n'\mathbf{k}'$. The energy dependence of the quantities plotted in Fig. 3 comes almost entirely from $\chi_{n'\mathbf{k}'}$, as the matrix elements themselves have a marginal energy dependence. In order to show how the reduction of Coulomb repulsion takes place, we emphasize in the lower panel of Fig. 3 the region corresponding to low matrix elements (on a linear scale). We see how, when Δ becomes negative, the Coulomb interaction actually gives a constructive contribution due to the minus sign in Eq. (24). Although the negative values are much smaller (by almost 3 orders of magnitude) than the positive ones, the corresponding energy range is much larger, resulting in the well-known, substantial reduction of the effective Coulomb contribution. The most important energy region is located in between 0.50 and 3 eV below E_F, in particular due to the strong intraband σ–σ matrix

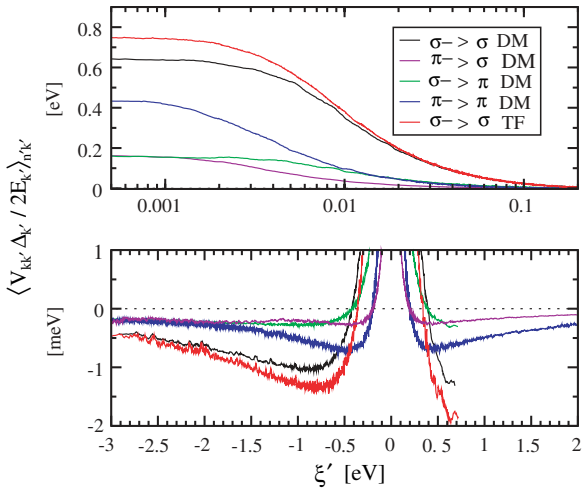

Fig. 3. Electronic repulsion contributions to the gap equation (see Eq. (24)), at an arbitrary $\mathbf{k}$, averaged over $\mathbf{k}'$ and bands on isoenergy surfaces, but keeping the σ, π distinction.

elements. The interband contribution from π bands (violet in Fig. 3), on the other hand, is considerably smaller, which is obviously the case also for the σ contribution to Δ_π (green in Fig. 3). Summing up over $n'\mathbf{k}'$, the negative contribution to Δ_σ coming from the (positive gap) region of the σ Fermi surface overcomes by a factor of ≈7 the contribution coming from the corresponding π region.

Finally, it is also interesting to investigate the importance of local field (LF) effects on the superconducting properties of MgB_2. It turns out that using a diagonal Thomas–Fermi screening (which completely neglects LF's) the σ–σ matrix elements increase by roughly 15% (red in Fig. 3), while the σ–π and π–π terms remain basically unchanged. As a consequence, neglecting LF effects leads to a marginal (≈4%) decrease of Δ_π, but decreases significantly Δ_σ (by about 14%). The different behavior of Δ_σ and Δ_π can be understood quite naturally: LF corrections imply a better screened interaction among electrons when they are located in a high density region inside the unit cell. This is precisely the case of the σ bands. On the other hand, the π bands are more delocalized – the electrons reside in the interstitial region – and are therefore reasonably described by diagonal screening. A result analogue to Thomas–Fermi screening is obtained using diagonal RPA, i.e. with $\epsilon^{-1}(\boldsymbol{q}, \boldsymbol{G} \neq \boldsymbol{G}') = 0$. A similar analysis on the LF effects also applies to the SC properties of CaC_6 [45].

In this communication, a recently developed ab initio theory of superconductivity is applied to MgB_2. The calculated value of T_c, the two gaps, as well as the specific heat as a function of temperature are in very good agreement with experiment. We stress the predictive power of the approach presented: being, by its very nature, a fully ab initio approach, it does not require semi-phenomenological parameters, such as μ^*. Nevertheless, it is able to reproduce with good accuracy superconducting properties, up to now out of reach of first-principles calculations. Furthermore, our calculations allow for a detailed analysis of the contribution of the Coulomb repulsion to the superconducting gap, opening the way to tailoring the electronic properties of real materials in order to optimize superconducting features.

Acknowledgements

The authors thank Giovanni Ummarino for helpful discussions and for providing results from Eliashberg calculations. This work was supported by the Italian MIUR under the projects PRIN 2006021741 and PON-CyberSar, by the Deutsche Forschungsgemeischaft within the program SPP 1145, by the EXC!TiNG Research and Training Network of the European Union, and by the NANOQUANTA NOE. We also acknowledge financial support by INFM (through a computing grant at Cineca, Bologna, Italy).

References

[1] H. Suhl, B.T. Matthias, L.R. Walker, Phys. Rev. Lett. 3 (1959) 552.
[2] G.M. Eliashberg, Sov. Phys. JETP 11 (1960) 696.
[3] G. Profeta et al., Phys. Rev. Lett. 96 (2006) 047003.
[4] R.M. Dreizler, E.K.U. Gross, Density Functional Theory, Springer Verlag, Berlin, 1990.
[5] P. Hohenberg, W. Kohn, Phys. Rev. 136 (1964) B864.
[6] G. Vignale, Mark Rasolt, Phys. Rev. Lett. 59 (1987) 2360.
[7] G. Vignale, Mark Rasolt, Phys. Rev. B 37 (1988) 10685.
[8] L.N. Oliveira, E.K.U. Gross, W. Kohn, Phys. Rev. Lett. 60 (1988) 2430.
[9] T. Kreibich, E.K.U. Gross, Phys. Rev. Lett. 86 (2001) 2984.
[10] N.D. Mermin, Phys. Rev. 137 (1965) A1441.
[11] N.N. Bogoliubov, Sov. Phys. JETP 7 (1958) 41.
[12] M. Lüders, M.A.L. Marques, N.N. Lathiotakis, A. Floris, G. Profeta, L. Fast, A. Continenza, S. Massidda, E.K.U. Gross, Phys. Rev. B 72 (2005) 024545.
[13] M.A.L. Marques, M. Lüders, N.N. Lathiotakis, G. Profeta, A. Floris, L. Fast, A. Continenza, E.K.U. Gross, S. Massidda, Phys. Rev. B 72 (2005) 024546.
[14] E.K.U. Gross, Stefan Kurth, Int. J. Quantum Chem. Symp. 25 (1991) 289.
[15] D.D. Koelling, J.H. Wood, J. Comput. Phys. 67 (1986) 253.
[16] W.E. Pickett, H. Krakauer, P.B. Allen, Phys. Rev. B 38 (1988) 2721.
[17] J. Kortus et al., Phys. Rev. Lett. 86 (2001) 4656.
[18] J.M. An, W.E. Pickett, Phys. Rev. Lett. 86 (2001) 4366.
[19] Y. Kong et al., Phys. Rev. B 64 (2001) 020501.
[20] K.P. Bohnen, R. Heid, B. Renker, Phys. Rev. Lett. 86 (2001) 5771.
[21] M. Iavarone et al., Phys. Rev. Lett. 89 (2002) 187002.
[22] P. Szabo et al., Phys. Rev. Lett. 87 (2002) 137005.
[23] H. Schmidt et al., Phys. Rev. Lett. 88 (2002) 127002.
[24] R.S. Gonnelli et al., Phys. Rev. Lett. 89 (2002) 247004.
[25] F. Giubileo et al., Phys. Rev. Lett. 87 (2001) 177008.
[26] M. Putti et al., Phys. Rev. B 68 (2003) 094514.
[27] F. Bouquet et al., Phys. Rev. Lett. 87 (2001) 47001.
[28] H.D. Yang et al., Phys. Rev. Lett. 87 (2001) 167003.
[29] H.J. Choi et al., Phys. Rev. B 66 (2002) 020513.
[30] H.J. Choi et al., Nature 418 (2002) 758.
[31] H.J. Choi et al., Phys. Rev. B 73 (2006) 104520.
[32] P.P. Singh, Phys. Rev. Lett. 97 (2006) 247002.
[33] A.Y. Liu, I.I. Mazin, J. Kortus, Phys. Rev. Lett. 87 (2001) 087005.
[34] I.I. Mazin et al., Phys. Rev. B 69 (2004) 056501.
[35] C.-Y. Moon et al., Phys. Rev. B 70 (2004) 104522.
[36] A.A. Golubov et al., J. Phys.: Condens. Matter 14 (2002) 1353.
[37] S. Baroni, S. de Gironcoli, A. Dal Corso, P. Giannozzi, Rev. Mod. Phys. 73 (2001) 515.
[38] Plane-Wave Self-Consistent-Field (PWSCF) code. <http://www.pwscf.org/>.
[39] J.P. Perdew, K. Burke, M. Ernzerhof, Phys. Rev. Lett. 77 (1996) 3865.
[40] D. Vanderbilt, Phys. Rev. B 41 (1990) 7892.
[41] A. Junod et al., Physica C 388–389 (2003) 107.
[42] A. Marini, SELF code. <www.fisica.uniroma2.it/~self/>.
[43] A. Floris, G. Profeta, N.N. Lathiotakis, M. Lüders, M.A.L. Marques, C. Franchini, E.K.U. Gross, A. Continenza, S. Massidda, Phys. Rev. Lett. 94 (2005) 037004.
[44] M.S. Hybertsen, S.G. Louie, Phys. Rev. B 37 (1988) 2733.
[45] A. Sanna, G. Profeta, A. Floris, A. Marini, E.K.U. Gross, S. Massidda, Phys. Rev. B 75 (2007) 020511.
[46] Taking only the nuclear density would lead to a system of strictly non-interacting nuclei which obviously would give rise to non-dispersive, hence unrealistic, phonons.
[47] The $T_c = 55$ K reported by Choi et al. [32] obtained with the harmonic $\lambda = 0.73$ and an isotropic $\mu^* = 0.12$ would probably reduce to T_c^{exp} using a consistent $\mu^*_{nn'}$ matrix.